

Understanding and Evaluating Human Preferences for AI Generated Images with Instruction Tuning

Jiarui Wang¹, Huiyu Duan^{1,2}, Guangtao Zhai^{1,2}, Xionghuo Min^{1*},

¹Institute of Image Communication and Network Engineering,

² MoE Key Lab of Artificial Intelligence, AI Institute,
Shanghai Jiao Tong University, Shanghai, China

Abstract—Artificial Intelligence Generated Content (AIGC) has grown rapidly in recent years, among which AI-based image generation has gained widespread attention due to its efficient and imaginative image creation ability. However, AI-generated Images (AIGIs) may not satisfy human preferences due to their unique distortions, which highlights the necessity to understand and evaluate human preferences for AIGIs. To this end, in this paper, we first establish a novel Image Quality Assessment (IQA) database for AIGIs, termed AIGCIQA2023+, which provides human visual preference scores and detailed preference explanations from three perspectives including quality, authenticity, and correspondence. Then, based on the constructed AIGCIQA2023+ database, this paper presents a MINT-IQA model to evaluate and explain human preferences for AIGIs from Multi-perspectives with Instruction Tuning. Specifically, the MINT-IQA model first learn and evaluate human preferences for AI-generated Images from multi-perspectives, then via the vision-language instruction tuning strategy, MINT-IQA attains powerful understanding and explanation ability for human visual preference on AIGIs, which can be used for feedback to further improve the assessment capabilities. Extensive experimental results demonstrate that the proposed MINT-IQA model achieves state-of-the-art performance in understanding and evaluating human visual preferences for AIGIs, and the proposed model also achieves competing results on traditional IQA tasks compared with state-of-the-art IQA models. The AIGCIQA2023+ database and MINT-IQA model will be released to facilitate future research on <https://github.com/IntMeGroup/MINT-IQA>

Index Terms—Artificial intelligence generated content (AIGC), image quality assessment (IQA), human visual preference, multiple perspectives, instruction tuning

I. INTRODUCTION

Artificial Intelligence Generated Content (AIGC) refers to the content generated with the assistance of AI, including texts, images, audios, *etc.* As an important part of AIGC, AI Generated Images (AIGIs) have gained significant attention due to their broad application prospects, thus, many AI-based image generation methods have been proposed in recent years, such as DALLE [1], Stable-diffusion [2], Unidiffuser [3], *etc.* However, due to the limitations of model capacity, computing overhead, and human-AI interaction gap, *etc.*, not all generated images can satisfy users' requirements, and many AIGIs do not conform to human visual preferences or expectations. Unlike common image content, such as Natural Scene Images (NSIs) [4], Screen Content Images (SCIs) [5] *etc.*, which generally encounters common degradations such as noise, blur,

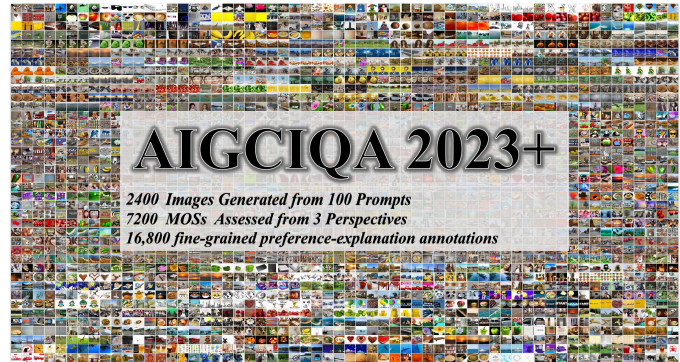


Fig. 1. We present AIGCIQA2023+, a large-scale dataset that includes 2400 images generated from 100 prompts, 7200 MOSs from 3 perspectives, and 16,800 fine-grained preference-explanation annotations.

compression [6]–[8], AIGIs exhibit unique distortions including unreal structures, unreasonable component combinations, *etc.* [9]–[11] Moreover, for text-to-image generation methods, the generated images may not accurately correspond to the semantics of the text prompts or may not meet the expectations of users [12], [13].

Given these challenges, there is an urgent need to study and model human visual preferences and expectations for AIGIs, which can be used to monitor the quality of generated images, filter unexpected images, or even feedback to refine and improve the generation capability of AI models [14]. To this end, several Image Quality Assessment (IQA) databases for AIGIs such as ImageReward [15], AGIQA-3K [16], AIGCIQA2023 [17], *etc.*, have been proposed to characterize the human visual preferences for AIGIs by scoring or ranking these images. However, these works lack fine-grained preference explanations for AIGIs, which makes it hard to understand corresponding human visual preferences and carry out adaptive model/data adjustments for the generation methods.

Furthermore, several evaluation metrics have been proposed for the objective evaluation of AIGIs. Inception Score (IS) [18], Fréchet Inception Distance (FID) [19], *etc.*, have been widely used to evaluate the authenticity of the generated images. However, these methods can not evaluate the authenticity of an individual generated image, and besides the authenticity properties, they cannot measure other human preference attributes such as quality and text-image correspondence. Additionally, Language-image pre-training techniques such as CLIP [20], BLIP [21], *etc.*, have been widely used to evaluate the text-image correspondence recently, which ignores the

*Corresponding Author.

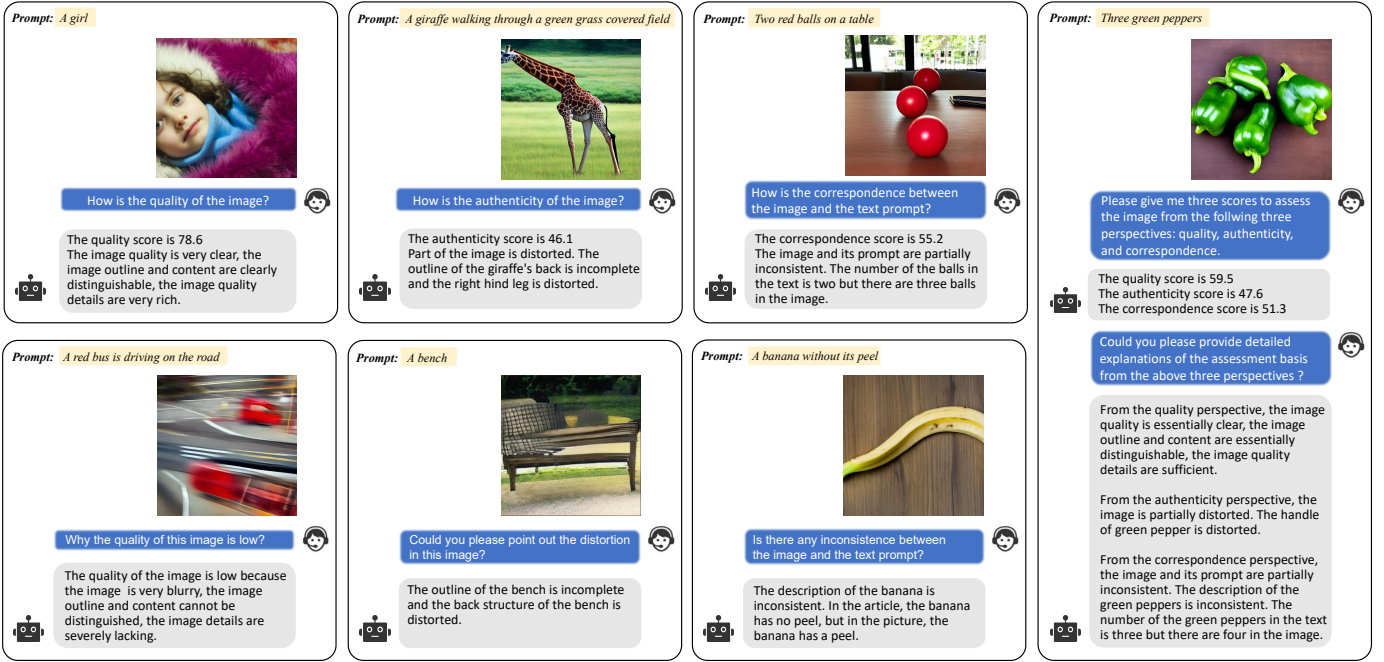


Fig. 2. Examples generated by our MINT-IQA model, demonstrating its diverse capabilities including image quality assessment from multiple perspectives, abundant degradation-aware visual question answering, comprehensive human visual preference explaining, *etc.*

visual experience attribute of AIGIs. Therefore, it is necessary to design a more comprehensive AIGI preference assessment model, which can evaluate both visual experience and text-image correspondence.

To address the aforementioned challenges, in this paper, we first extend the previous AIGCIQA2023 database [17] to AIGCIQA2023+, towards better understanding and evaluating human preferences for AIGIs, and then propose a novel method, termed **MINT-IQA**, towards automatically evaluating and explaining the visual preference and expectation attributes for AIGIs from **Multi-perspectives with INstruction Tuning**. Specifically, as shown in Fig. 1, the established AIGCIQA2023+ contains 2400 AIGIs generated using 6 AIGI models based on 100 text prompts, 7,200 Mean Opinion Scores (MOSs) and 16,800 detailed preference-explanation annotations for these AIGIs. The evaluation perspectives include quality, authenticity, and text-image correspondence. We further propose a MINT-IQA model, which allows for a more comprehensive evaluation of the human preferences for AIGIs from multi-perspectives, resulting in state-of-the-art performance on AIGC IQA databases. To further enhance the degradation understanding and explanation capabilities of our model, we adopt the vision-language instruction tuning strategy, and fine-tune the MINT-IQA model based on the AIGCIQA2023+ database. This approach effectively leverages the frozen Large Language Model (LLM) to provide detailed explanations of the human preference basis for each AIGI as shown in Fig. 2, which can be used for feedback to further improve the assessment capabilities as shown in Section V. Additionally, MINT-IQA model also achieves the best performance on traditional IQA databases, which further demonstrates its generality in understanding and evaluating human preferences.

The main contributions of this paper can be summarized as follows:

- We establish an AI generated image quality assessment database, termed AIGCIQA2023+, to conduct comprehensive understanding and evaluation research on human visual preferences for AIGIs.
- We propose a MINT-IQA model, which integrates text and image information via Q-Former to evaluate the human visual preference from multiple perspectives including quality, authenticity, and text-image correspondence.
- We utilize the vision-language instruction tuning strategy to enable MINT-IQA to better understand and explain human visual preference on AIGIs, which can be used to further improve the evaluation ability.
- Extensive experimental results demonstrate that our proposed MINT-IQA model achieves state-of-the-art performance on both AIGC IQA databases and traditional IQA databases, and attains comprehensive understanding and explanation capabilities for human visual preference of AIGIs.

II. RELATED WORK

A. Image Quality Assessment Databases

Many IQA databases have been established in the literature [27]–[29]. As shown in Table I, according to the image acquisition method, they can be categorized into two types: (1) traditional IQA databases and (2) AIGC IQA databases. Traditional IQA databases consist of natural images with realistic camera distortions such as noise, blur, compression, *etc.* CID2013 [22] is a small database consists of 585 realistically blurred pictures taken by 79 cameras. KonIQ-10k [30] and SPAQ [24] expand the data scale and cover a wide range of scene categories. AVA [25] is a large-scale database constructed for aesthetic image quality assessment. Recently, the development of text-to-image generative models have led to an explosion of AI-generated images. Thus many AIGC IQA databases have also been constructed, which contain generated images with unique distortions including unreal

COMPARISON OF IMAGE QUALITY ASSESSMENT DATABASES, INCLUDING TRADITIONAL IQA DATABASES AND AIGC IQA DATABASES.

Type	Database	Score	Preference annotation	Image	Ratings	Explanations
Traditional IQA Databases	CID2013 [22]	Rating	Overall	480	14,880	No
	KonIQ-10k [23]	MOS	Overall	10,073	1,208,760	No
	SPAQ [24]	MOS	Overall	11,125	55,625	No
	AVA [25]	Rating	Overall	255,000	53,550,000	No
AIGC IQA Databases	DiffusionDB [26]	No	No	1,819,808	0	No
	HPS [9]	Preference	Overall	98,807	98,807	No
	Pick-A-Pic [14]	Preference	Overall	500,000	500,000	No
	ImageReward [15]	Ranking	Overall	136,892	410,676	No
	AGIQA-3K [16]	MOS	Perception, alignment	2,982	125,244	No
	AIGCIQA2023 [17]	MOS	Quality, authenticity, correspondence	2,400	201,600	No
	AIGCIQA2023+	MOS	Quality, authenticity, correspondence	2,400	201,600	16,800

structures, unreasonable component combinations, *etc.* DiffusionDB [26] is a large-scale database containing over 1.8 million text-image pairs without score-specific annotations. Pick-A-Pic [14] and HPS [9] provide subjective annotations of human preferences by selecting the most preferred one among a group or a pair of AIGIs. ImageReward [15] contains preference ranking annotations for AIGIs. The aforementioned AIGC IQA databases only evaluate the AIGIs from the overall dimension, which cannot reflect and characterize complex human visual preferences for AIGIs. AGIQA-3K [16] refines the rating granularity by scoring two dimensions including perception and alignment. Our preliminary AIGCIQA2023 database [17] contains subjective quality ratings from three dimensions including quality, authenticity, and correspondence. However, the aforementioned works lack detailed annotations of the human preference for AIGIs, which motivates us to further extend the AIGCIQA2023 database to include language annotations.

B. Image Quality Assessment Models

Image quality assessment algorithms aim to objectively and quantitatively evaluate the perceptual quality of images. Based on different feature extraction and evaluation methods, current popular models for image quality assessment can be classified into three categories: (1) Handcrafted-based models, including: NIQE [31], BRISQUE [32], QAC [33], BMPRI [34], HOSA [35], BPRI [36], HIGRADE [37], *etc.* These models generally extract features based on prior knowledge related to image quality. (2) Deep learning-based models, including: CNNIQA [38], DBCNN [39], WaDIQaM-NR [40], StairIQA [41], *etc.* These models characterize quality-aware information by training deep neural networks using labeled data. (3) With the popularity of text-to-image generation, many vision-language pre-training models have been adopted to evaluate the text-image alignment, including: CLIP [20], BLIP [21], FLIP [42], Aesthetic [43], HPS [9], PickScore [14], ImageReward [15], StairReward [16], *etc.* These models are often used for evaluating generated images based on its text prompt considering a mixture of elements such as text-image alignment, fidelity, aesthetics, *etc.*

The aforementioned models can only evaluate a single-dimension preference for AIGIs, which lacks the ability to conduct a comprehensive assessment from multiple perspectives. This motivates us to propose a unified model to evaluate AIGIs from multiple dimensions.

III. DATABASE CONSTRUCTION AND ANALYSIS

This work focuses on understanding and evaluating human preferences for AI-generated images, therefore it is necessary



Fig. 3. Rating comparisons between three perspectives. (a) The quality score of the left image is higher, but other two scores are lower. (b) The authenticity score of the left image is higher, but other two scores are lower. (c) The correspondence score of the left image is higher, but other two scores are lower.

to construct a database that provides various AI-generated images with accurate human preference scores and detailed explanations for evaluation factors. In order to better understand human preferences for AIGIs, we propose to disentangle the human visual experience of AIGIs into three perspectives, including quality, authenticity, and correspondence, and then conduct scoring and interpretation. “Quality” evaluates an AIGI from the visual quality attribute considering the brightness, colorfulness, clarity, *etc.*, “authenticity” evaluates the reality-degree attribute of an AIGI including naturalness, harmonious, *etc.*, “correspondence” assesses the relevance attribute between an AIGI and its prompt. As shown in Fig. 3, different dimensions can reflect different human preference characteristics, which further strength the importance of evaluating AIGIs from multiple perspectives. Overall, our constructed AIGCIQA2023+ dataset contains 2,400 AI-generated images with 7,200 corresponding MOSs evaluated from three perspectives and 16,800 detailed interpretations of evaluation criteria. Detailed subjective experimental procedures are described as follows.

A. AIGI Collection

We adopt six latest text-to-image generative models, including Glide [44], Lafite [45], DALLE [46], Stable-diffusion [47], Unidiffuser [3], Controlnet [48], to produce AIGIs by using open source code and default weights. To ensure content diversity and catch up with the practical application requirements, we collect diverse texts from the PartiPrompts website [49] as the prompts for AI-based image generation. The text prompts can be simple, allowing generative models to produce imaginative results. They can also be complex, which raises the challenge for generative models. We select 10 scene

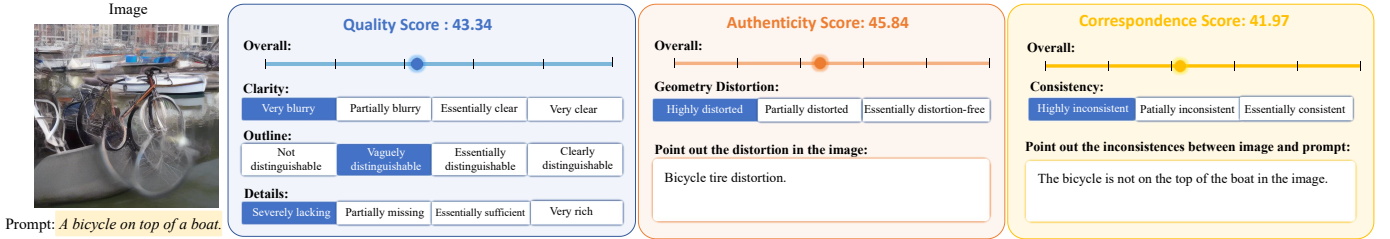


Fig. 4. Illustration of the subjective assessment interface. The subjects are instructed to make fine-grained assessments and annotations by clicking the checkboxes and give further detailed explanations by inputting text descriptions.

categories from the prompt set, and each scene contains 10 challenge categories. Overall, we collect 100 text prompts (10 scene categories \times 10 challenge categories) from PartiPrompts [49]. Based on the selected prompts, we generate 4 different images for each generative model. Therefore, the constructed database totally contains 2400 AIGIs (4 images \times 6 models \times 100 prompts).

B. Subjective Experiment Setup

Based on the collected AIGIs, we further conduct a subjective experiment following the guidelines of ITU-R BT.500-14 [50], to obtain subjective quality ratings from the perspectives of quality, authenticity, and text-image correspondence. The detailed explanations for the three perspectives can be found above in Section III. Moreover, to obtain fine-grained preference-related annotations, subjects are instructed to give detailed explanations by finishing the fill-in-the-blank questions. Specifically, for the quality perspective, the subjects are asked to give detailed description choices for the degree of image clarity, the outline and content of the image, and the richness of details. As for the authenticity perspective, subjects are instructed to assess the distortion severity and point out the specific distorted part of each AIGI. To evaluate the text-image correspondence, subjects are instructed to consider whether there is any inconsistency between the image content and its text prompt and then input detailed explanations through typing. In our subjective experiment, there are five single-choice questions designed. Each question corresponds to a factor that influences human preference for each AIGI. We provide several choices to define the level of each factor. For image clarity, we divide it into four levels, including: very blurry, partially blurry, essentially clear, and very clear. Similarly, for the factors of the image outline and details, we also divide them into four levels. Furthermore, the geometry distortion and the text-image consistency are divided into three levels, including: highly (distorted / inconsistent), partially (distorted / inconsistent), and essentially (distortion-free / consistent).

The AIGIs are presented in a random order on an iMac monitor with a resolution of 4096×2304 , using an interface designed with Python Tkinter as shown in Fig. 4. The interface allows viewers to browse the previous and next AIGIs, and evaluate them by scoring within the range from 0 to 5 as well as providing fine-grained explanations. A total of 76 graduate students participate in the experiment. The subjects are seated at a distance of around 60 cm in a laboratory environment with normal indoor lighting. The subjects are provided with detailed evaluation criteria and trained before the formal experiment to be familiar with the experiment. Individuals who demonstrate low agreement accuracy are excluded from the experiment.

Finally, we collect 84 (28 subjects \times 3 perspectives) ratings and an average of 7 preference descriptions for each AIGI, resulting in a total number of 201,600 (28 \times 3 \times 2400) quality ratings and 16,800 (7 \times 2,400) detailed explanations.

C. Subjective Rating Processing

We follow the suggestions recommended by ITU to conduct the outlier detection and subject rejection. The score rejection rate is 2%. In order to obtain the MOS for an AIGI, we first convert the raw ratings into Z-scores, then linearly scale them to the range [0, 100] as follows:

$$z_{ij} = \frac{r_{ij} - \mu_j}{\sigma_j}, \quad z'_{ij} = \frac{100(z_{ij} + 3)}{6}, \quad (1)$$

$$\mu_j = \frac{1}{N_i} \sum_{i=1}^{N_i} r_{ij}, \quad \sigma_j = \sqrt{\frac{1}{N_i - 1} \sum_{i=1}^{N_i} (r_{ij} - \mu_j)^2}, \quad (2)$$

where r_{ij} is the raw ratings given by the i -th subject to the j -th image. N_i is the number of images judged by subject i . Next, the mean opinion score (MOS) of the image j is computed by averaging the rescaled z-scores as follows:

$$MOS_j = \frac{1}{M} \sum_{i=1}^M z'_{ij} \quad (3)$$

where MOS_j indicates the MOS for the j -th AIGI, M is the number of valid subjects, and z'_{ij} are the rescaled z-scores.

D. Question Answering Pair Generation

In order to enable the detailed human preference explanation ability for an IQA model, we collect numerous question-answering pairs tailored for instruction tuning. Some of the questions are consistent with the setup questions in our subjective experiment, and some are extended based on the degradation or quality-related labels. The extended question-answering pairs are generated with the help of large language models (LLMs). Specifically, we feed the collected quality labels and detailed explanations into LLMs, then prompt LLMs to ask questions for these answers. This step can greatly expand the scale of VQA pairs. Fig. 5 fine-grained human preference annotations, we can improve the perceptual explanation capability of LLMs and further improve the performance of IQA models.

E. Human Annotation Analysis

We first analyze the subjective quality rating and MOS distribution from the perspectives of quality, authenticity, text-image correspondence respectively. As shown in Fig. 6, the images in AIGCIQA2023+ database cover a wide range of

(1) Prompt: Three green peppers

(2) Generated image



(3) Collected preference annotations

Quality (47.26)

Clarity: Partially blurry

Outline: Vaguely distinguishable

Details: Essentially sufficient

Authenticity (45.81)

Geometry Distortion: Partially distorted

Annotation: The handle of green pepper is distorted.

Correspondence (49.65)

Consistency: Partially inconsistent

Annotation: The description of the green peppers is inconsistent. The number of the green peppers in the text is three but there are four in the image.

(4) Generated question-answering pairs

<p>Question 1: How is the quality of the image? Answer 1: The quality score is 47.26, the image is partially blurry, the image outline and content are vaguely distinguishable, the image quality details are essentially sufficient.</p> <p>Question 2: Please assess the image from quality perspective. Answer 2: The quality score is 47.26, the image is partially blurry, the image outline and content are vaguely distinguishable, the image quality details are essentially sufficient.</p> <p>Question 3: Why the quality of the image is low? Answer 3: The image is partially blurry, the image outline and content are vaguely distinguishable, the image quality details are essentially sufficient.</p> <p>Question 4: How is the clarity of the image? Answer 4: The image is partially blurry.</p> <p>Question 5: How is the outline of the image? Answer 5: The image outline and content are vaguely distinguishable.</p> <p>Question 6: How is the detail of the image? Answer 6: The image quality details are essentially sufficient.</p>	<p>Question 7: How is the authenticity of the image? Answer 7: The authenticity score is 45.81, the image is partially distorted. The handle of green pepper is distorted.</p> <p>Question 8: Please assess the image from authenticity perspective. Answer 8: The quality score is 45.81, the image is partially distorted. The handle of green pepper is distorted.</p> <p>Question 9: Why the authenticity of the image is low? Answer 9: The image is partially distorted. The handle of green pepper is distorted.</p> <p>Question 10: Could you please point out the geometry distortion in this image? Answer 10: The handle of green pepper is distorted.</p> <p>Question 11: How is the distortion of the image? Answer 11: The image is partially distorted. The handle of green pepper is distorted.</p>	<p>Question 12: How is the correspondence between the image and text? Answer 12: The correspondence score is 49.65, the image and its prompt are partially inconsistent. The description of the green peppers is inconsistent. The number of the green peppers in the text is three but there are four in the image.</p> <p>Question 13: Please assess the image from correspondence perspective. Answer 13: The correspondence score is 49.65, the image and its prompt are partially inconsistent. The description of the green peppers is inconsistent. The number of the green peppers in the text is three but there are four in the image.</p> <p>Question 14: Is there any inconsistency between the image and the text? Answer 14: The description of the green peppers is inconsistent. The number of the ball in the text is three but there are four green peppers in the image.</p> <p>Question 15: Is the generated image and the text aligned? Answer 15: The image and its prompt are partially inconsistent.</p>
<p>Question 16: Give me three scores to assess the image from the following three perspectives: quality, authenticity, and correspondences. Answer 16: The quality score is 47.26. The authenticity score is 45.81. The correspondence score is 49.65</p>		

Fig. 5. Illustration of the generated visual question-answering pairs for instruction tuning.

perceptual quality. We further analyze the distributions of fine-grained annotations. Fig. 7 demonstrates the distribution of fine-grained annotations for all models, and Fig. 8 further shows the distribution of fine-grained annotations for different generation models including Glide [44], Lafite [45], Unidiffuser [3], Stable-diffusion [47], Controlnet [48], DALLE [46]. It can be observed that the performance of DALLE [46] is the best among all the six AIGI models. The performance of Glide [44] and Lafite [45] is relatively poor compared to other models in terms of the fine-grained assessment. Besides, Lafite [45] is better than Glide [44] in terms of text-image consistency, but far worse than Glide [44] in terms of the authenticity perspective. This also manifests that different AIGI models have different defects, which further illustrates the importance of evaluating AIGIs from multiple perspectives. And our analysis can help users choose appropriate AIGI models according to the different preference emphasis.

IV. PROPOSED METHOD

We propose a MINT-IQA model to evaluate and explain human preferences from multiple perspectives with instruction tuning, which contains two main functions: (1) predicting human preference scores for AIGIs from multiple perspectives; (2) providing detailed explanations of the factors influencing human preference according to the questions. The network

architecture of MINT-IQA is demonstrated in Fig. 9. Specifically, the MINT-IQA model consists of three parts: (1) Given prompt and its generated image, we first use LLMs to segment the prompt to be more understandable, then encode the refined prompt and the generated image into text tokens and image embeddings using a text encoder and a image encoder, respectively. (2) For learning to evaluate the quality of the image, the extracted text and image features are interacted with each other through a cross-modal querying transformer (Q-Former) to capture preference representations which are separately mapped to various preference scores through different regressors. (3) To further understand and explain the evaluation process, another Q-Former is applied before a frozen LLM to perform instruction tuning and output answers for a given instruction question. Detailed methods are given as follows.

A. Learning and Evaluating

Given an AIGI and its corresponding prompt, we first segment the prompt to be more understandable and explicit through a LLM. Then we use a text encoder and an image encoder for textual and visual feature extraction. The extracted text and image features are interacted with each other through a cross-modal Querying Transformer (Q-Former) to learn multimodal quality representations which are then given to

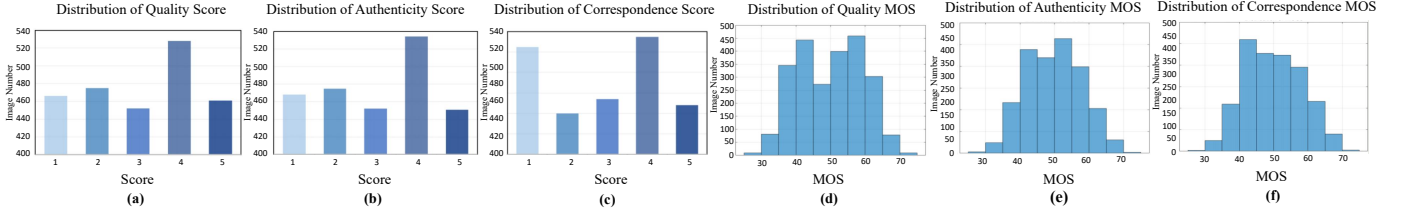


Fig. 6. (a) Distribution of the quality scores. (b) Distribution of the authenticity scores. (c) Distribution of the correspondence scores. (d) Distribution of the quality MOSs. (e) Distribution of the authenticity MOSs. (f) Distribution of the text-image correspondence MOSs.

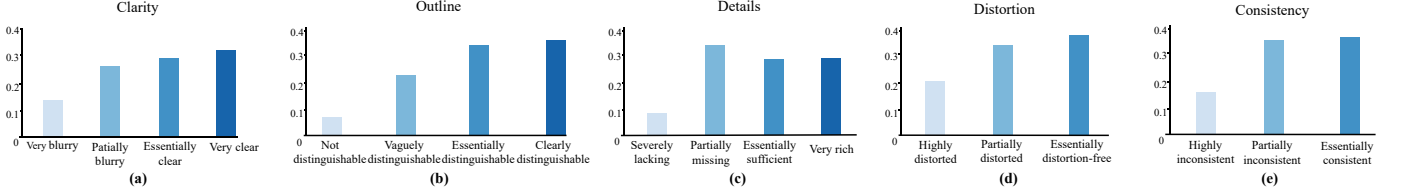


Fig. 7. Distribution of fine-grained annotations. (a) Distribution of the clarity. (b) Distribution of the outline recognizability. (c) Distribution of the richness of details. (d) Distribution of the geometry distortion. (e) Distribution of the text-image consistency.

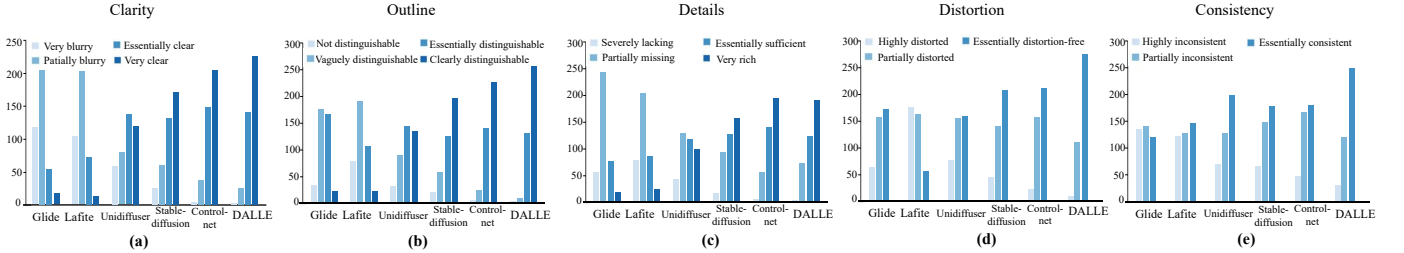


Fig. 8. Distribution of fine-grained annotations for different generation models including Glide [44], Lafite [45], Unidiffuser [3], Stable-diffusion [47], Controlnet [48], DALLE [46]. (a) Distribution of the clarity. (b) Distribution of the outline recognizability. (c) Distribution of the richness of details. (d) Distribution of the geometry distortion. (e) Distribution of the text-image consistency.

regressors to predict human preference scores from multiple perspectives.

1) *Prompt Segmentation*: The content and length of the input prompt are of great significance in the text-image correspondence performance evaluation. The information provided by the original prompt may not be cohesive or meaningful enough, thus may lead to poor performance on the evaluation of AIGIs, particularly in terms of text-image correspondence. To address this issue, we apply a “raw prompt + LLM-refined prompt” mechanism to make the text more understandable for text models. Specifically, we utilize a LLM to transform text prompts into three task-specific annotations including “style”, “content”, and “atmosphere”. “Style” words describe the whole image style, including painting, artistic, realistic, fashion, texture, fiction, *etc.* If the original input text does not have style cues, the default style is “realistic”. “Content” words are nouns with adjectives describing the image content. “Atmosphere” words refer to the emotional and psychological elements associated with the image, including mood and feeling conveyed by the scene. All of these three items lying after the raw prompt are crucial to the assessment of text-image correspondence.

2) *Feature Extraction*: The feature extraction part consists of an image encoder and a text encoder. The input image is transformed into image embeddings through the image encoder while the input text prompt is encoded into text tokens through a text encoder. The encoders are initialized with pre-trained weights and are partially frozen to reduce computation costs. In practice, we utilize the frozen visual encoder ViT-G/14 from EVA-CLIP [51] and the text encoder from BLIP [21], which differs from the text and image encoders employed in CLIP [20].

3) *Multimodal Representation Learning*: Based on the extracted independent text and image features, a multi-modal Q-Former is applied to learn and extract multi-modal preference-aware representations, which employs a set of learnable query vectors to interact with image embeddings and text tokens using cross-attention and self-attention [52], [53]. Specifically, these learnable queries interact with each other as well as the text-tokens through self-attention layers and interact with the image embeddings through cross-attention layers. Different from BLIP-2 [54], the Q-Former in our proposed model aims to extract the most informative quality-aware features from the partially frozen image and text encoders for the following regressors to output the desired scores consistent with human preferences from multiple perspectives.

4) *Score Regression*: After extracting quality-aware representations through the Q-Former, we map these features to the desired score spaces using the score regression module. Three score regressors are used for quality, authenticity, and text-image correspondence score regression, respectively. However, the number of the regressors can be increased or decreased according to the number of the evaluation dimensions of the corresponding database, not limited to the three perspectives as mentioned above. To reduce the model complexity, the structure and loss function of the regressors remain the same.

B. Understanding and Explaining with Instruction Tuning

To gain a deeper understanding of the human visual preference for AIGIs and provide more detailed explanations for the multi-dimensional evaluation principle, we implement another Q-Former for vision-language instruction tuning. It inherits quality-aware information from the previous Q-Former, interacting with instructions and image embeddings to extract

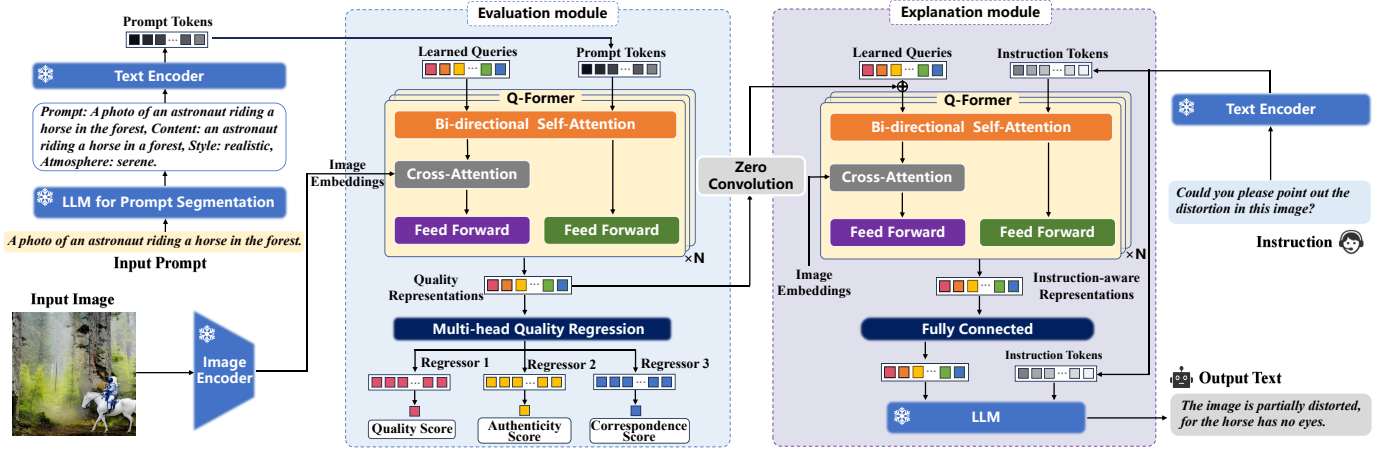


Fig. 9. An overview of the architecture of the proposed MINT-IQA model. The MINT-IQA model consists of three parts: (1) For a given prompt and its generated image, we first use LLMs to segment the prompt to be more understandable, then use a text encoder and an image encoder to extract text and image features, respectively. (2) The extracted text and image features are interacted with each other through a cross-modal Q-Former to capture preference-related representations which are then separately regressed to various preference scores. (3) To enable the preference-related explanation capability for MINT-IQA, the extracted preference representations are interacted with the extracted instruction features via another Q-Former to obtain instruction-aware representations, which are then fed into a LLM to give answers and explanations.

instruction-aware representations. Then we apply a LLM to perform representation-guided visual question answering according to the given instruction.

1) *Instruction-aware Representation Extraction*: We incorporate the quality representation queries obtained from the previous Q-Former into the initial input queries of the instruction tuning Q-Former. The two Q-Formers are connected through a zero convolution. The weights and biases of the zero convolution are initialized with zero but will be adjusted during the training process. By doing so, we can supplement the instruction tuning Q-Former with the quality-aware information from the first Q-Former, while avoiding adding initial noise to the pre-trained InstructBLIP [55] with the help of zero initialized convolution. The instruction information is also given to the Q-Former after being encoded by a text encoder, enabling the Q-Former to extract instruction-aware visual representations from the output of the image encoder through cross-attention.

2) *Representation-guided Visual Question Answering*: We perform representation-guided degradation-related visual question answering by connecting the output of the instruction tuned Q-Former to a frozen LLM. The frozen LLM adopted in our model is Vicuna [56], a recently released decoder-only LLM finetuned from LLaMA [57]. The connection part between the Q-Former and LLM is a fully-connected layer which adapts the instruction-aware visual representations to the input dimension of the LLM. Since the LLM is adapted to output different answers with instruction tuning, it can keep frozen to reduce computation while getting the ability of human visual preference explaining.

C. Training and Fine-tuning Strategy

The proposed model undergoes a three-stage training process: (1) score regression pretraining stage, (2) vision-to-language instruction tuning stage, (3) feedback from the understanding module to evaluating module. During the first stage, the Q-Former is pre-trained for vision-language representation learning and image quality score regression. In the second stage, we freeze the first Q-Former and initialize the instruction

tuning Q-Former with a pre-trained InstructBLIP [55] model and further fine-tune it on the AIGCIQA2023+ database. For the third stage, the output of the explanation module is feedback to the score regression module to further improve the performance.

1) *Score Regression Pre-training*: There are three types of image annotations in current AIGCIQA databases including MOS, pairs, and rankings. For the MOS input format, we simply use the $L1$ loss to optimize the training process. The loss function is formulated as follows:

$$\mathcal{L} = \frac{1}{N} \sum_{i=1}^N |Q_{\text{predict}}(i) - Q_{\text{label}}(i)| \quad (4)$$

where $Q_{\text{predict}}(i)$ is the score predicted by the regressor i and $Q_{\text{label}}(i)$ is the corresponding ground-truth MOS collected from subjective experiments, N is the total number of regressors used in the model. For the annotation format of pairs, we use the cross-entropy loss to optimize the network. Suppose $\{P_b, P_w\}$ is a pair of images for comparison and P_b is the better one while P_w is the worse, the loss function can be formulated as:

$$\mathcal{L}(\theta) = -\mathbb{E}_{(T, P_b, P_w) \sim \mathcal{D}} [\log(\sigma(f_{\theta}(T, P_b) - f_{\theta}(T, P_w)))] \quad (5)$$

where $f_{\theta}(T, P)$ is predicted preference score for prompt T and generated image P . For the ranking annotations, the images from the best to the worst can be denoted as P_1, P_2, \dots, P_k . We can arrange and combine them into the following pairs: $\{P_1, P_2\}, \{P_1, P_3\}, \dots, \{P_{k-1}, P_k\}$. If there are k ranking images with the same prompt T , we can obtain a maximum of C_k^2 comparison pairs. Then the cross-entropy loss function used for pair format can be applied for the ranking format.

2) *Vision-to-Language Instruction Tuning*: To further enhance the explanation capabilities of our model, we propose a vision-language instruction tuning strategy. We initialize the weights of the instruction tuning Q-Former with pretrained InstructBLIP [55], which empowers the model with initial ability of complex visual scene understanding. To further enhance the degradation-awareness capabilities of our model, we fine-tune it on our AIGCIQA2023+ database to adapt the

TABLE II

PERFORMANCE COMPARISONS OF THE STATE-OF-THE-ART IQA METHODS ON THE AIGCIQA2023+ DATABASE FROM THREE PERSPECTIVES. THE BEST PERFORMANCE RESULTS ARE MARKED IN RED AND THE SECOND-BEST PERFORMANCE RESULTS ARE MARKED IN BLUE.

Method	Quality			Authenticity			Correspondence			Average		
	SRCC	PLCC	KRCC	SRCC	PLCC	KRCC	SRCC	PLCC	KRCC	SRCC	PLCC	KRCC
NIQE [31]	0.5060	0.5218	0.3420	0.3715	0.3954	0.2453	0.3659	0.3485	0.2460	0.4145	0.4219	0.2778
QAC [33]	0.5328	0.5991	0.3644	0.4009	0.4428	0.2673	0.3526	0.4062	0.2414	0.4288	0.4827	0.2910
BRISQUE [32]	0.6239	0.6389	0.4291	0.4705	0.4796	0.3142	0.4219	0.4280	0.2865	0.5054	0.5155	0.3433
BPRI [36]	0.6301	0.6889	0.4307	0.4740	0.5207	0.3144	0.3946	0.4346	0.2657	0.4996	0.5481	0.3369
HOSA [35]	0.6317	0.6561	0.4311	0.4716	0.4985	0.3101	0.4101	0.4252	0.2765	0.5045	0.5266	0.3392
BMPRI [34]	0.6732	0.7492	0.4661	0.5273	0.5756	0.3554	0.4419	0.4827	0.3014	0.5475	0.6025	0.3743
Higrade-1 [37]	0.4849	0.4966	0.3220	0.4175	0.4181	0.2791	0.3319	0.3379	0.2207	0.4114	0.4175	0.2739
Higrade-2 [37]	0.2344	0.3189	0.1568	0.2654	0.3106	0.1742	0.1756	0.2144	0.1170	0.2251	0.2813	0.1493
CLIP Score [20]	0.2355	0.2629	0.2629	0.1456	0.0966	0.1752	0.2337	0.1578	0.2729	0.2049	0.1724	0.2370
BLIP Score [21]	0.3485	0.2319	0.3552	0.3191	0.2128	0.3275	0.3784	0.2576	0.3882	0.3487	0.2341	0.3570
FLIP Score [42]	0.3424	0.2287	0.3575	0.2287	0.1717	0.2670	0.3561	0.2427	0.3822	0.3091	0.2144	0.3356
Aesthetic Score [43]	0.5879	0.4057	0.5974	0.5087	0.3473	0.5162	0.4851	0.3299	0.4942	0.5272	0.3610	0.5359
ImageReward Score [15]	0.5153	0.5229	0.3507	0.4802	0.4836	0.3265	0.5870	0.5911	0.4094	0.5275	0.5325	0.3622
WaDIQaM-NR [40]	0.4447	0.4996	0.3036	0.3936	0.3906	0.2715	0.3027	0.2810	0.2057	0.3803	0.3904	0.2603
CNNIQA [38]	0.7160	0.7937	0.4955	0.5958	0.5734	0.4085	0.4758	0.4937	0.3313	0.5959	0.6203	0.4118
VGG16 [58]	0.7961	0.7973	0.5843	0.6660	0.6807	0.4813	0.6580	0.6417	0.4548	0.7067	0.7066	0.5068
VGG19 [58]	0.7733	0.8402	0.5376	0.6674	0.6565	0.4843	0.5799	0.5670	0.4090	0.6735	0.6879	0.4770
Resnet18 [59]	0.7583	0.7763	0.5360	0.6701	0.6528	0.4740	0.5979	0.5564	0.4165	0.6754	0.6618	0.4755
Resnet34 [59]	0.7229	0.7578	0.4835	0.5998	0.6285	0.4325	0.7058	0.7153	0.5111	0.6762	0.7005	0.4757
MUSIQ [60]	0.8421	0.8475	0.6338	0.7382	0.7278	0.5377	0.7381	0.7216	0.5418	0.7728	0.7656	0.5711
TreS [61]	0.8389	0.8640	0.6283	0.7480	0.7371	0.5511	0.7401	0.7188	0.5448	0.7757	0.7733	0.5747
CLIP-IQA+ [62]	0.8300	0.8405	0.6170	0.7325	0.7199	0.5265	0.6484	0.6424	0.4554	0.7370	0.7343	0.5330
MINT-IQA (Ours)	0.8801	0.8870	0.6841	0.8229	0.8127	0.6223	0.8226	0.8055	0.6231	0.8419	0.8351	0.6432

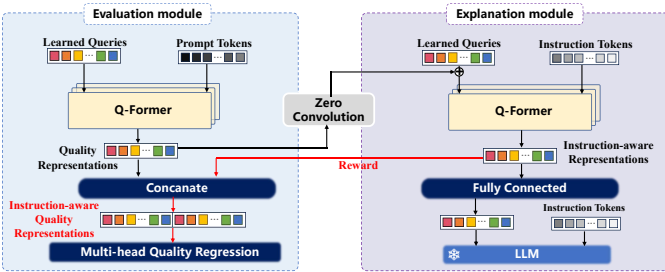


Fig. 10. Feedback from the explanation module to evaluation module. (Improvement in RED.)

frozen LLM to give fine-grained explanations for the quality assessment basis of each AIGI. The model is trained using the standard language modeling loss. We freeze the first Q-Former during training to reduce computational complexity and avoid affecting the previous score prediction procedure. This instruction tuning strategy enables the MINT-IQA model to further attain the powerful capability for human visual preference explanation while maintaining the original complex visual scene understanding ability.

3) *Feedback from the explanation module to evaluating module*: To further strengthen the connection between the two frameworks and help predict more accurate scores, we take the instruction-aware representations from the second framework as a reward. As shown in Fig. 10, we concatenate the instruction-aware representations and the quality-aware representations as the input for multi-head quality regression, and then fine-tune the three regressors respectively with corresponding instructions. For example, when finetuning the quality regressor, the instruction is “how is the quality of the image?”. The instruction-aware representations according to this instruction are highly quality-aware. Consequently, taking these representations from the second framework as a reward to the first framework leads to more accurate quality score prediction. As shown in Table XIV, the model gains better performance through the feedback.

V. EXPERIMENT

In this section, we conduct extensive experiments to evaluate the performance of our proposed model. We first present the experimental protocol in detail. Then we launch experiments to assess the IQA performance of our model compared to current state-of-the-art IQA models in predicting human preference based on three AIGC IQA databases and three traditional IQA databases. To quantitatively measure the accuracy of our model in explaining human preference for AIGIs, we propose Visual Question Answering Accuracy (VQA_{acc}) for the evaluation of the human preference explanation task. We launch further cross-dataset experiments to test the generalizability of proposed model. Finally, we conduct ablation experiments to evaluate the efficiency of our proposed components.

A. Experimental Protocol

We assess the performance of our proposed method on six IQA databases including three AIGC IQA databases (AIGCIQA2023 [17], AGIQA-3K [16], ImageReward [15]) and three traditional IQA databases (KonIQ-10k [23], SPAQ [24], AVA [25]). To evaluate the correlation between the predicted scores and the corresponding ground-truth MOSs, we utilize the following three correlation coefficients as performance evaluation criteria, including Spearman Rank Correlation Coefficient (SRCC), Pearson Linear Correlation Coefficient (PLCC), and Kendall’s Rank Correlation Coefficient (KRCC).

Some baseline results are evaluated by ourselves. For traditional handcrafted-based models, they are directly evaluated on the corresponding databases. For vision-language pre-training models, we simply load the pre-trained weights for inference. CLIP score and BLIP score are calculated directly as cosine similarity between text and image embeddings. For deep learning-based models, we use the same training and testing split as the previous literature. For our proposed model, the number of regressors in our model is flexible, corresponding

TABLE III

PERCEPTION METRIC PERFORMANCE COMPARISONS ON THE AGIQA-3K DATABASE. THE BEST RESULTS ARE MARKED IN RED AND THE SECOND RESULTS ARE MARKED IN BLUE.

Method	SRCC	PLCC	KRCC
CEIQ [63]	0.3228	0.4166	0.2220
DSIQA [64]	0.4955	0.5488	0.3403
NIQE [31]	0.5623	0.5171	0.3876
Sisblim [65]	0.5479	0.6477	0.3788
FID [19]	0.1733	0.1860	0.1158
ICS [66]	0.0931	0.0964	0.0626
KID [67]	0.1023	0.0786	0.0692
BMPRI [34]	0.6794	0.7912	0.4976
GMLF [68]	0.6987	0.8181	0.5119
Higrade [37]	0.6171	0.7056	0.4410
DBCNN [39]	0.8207	0.8759	0.6336
CLPIQA [20]	0.8426	0.8053	0.6468
CNNIQA [38]	0.7478	0.8469	0.5580
HyperNet [69]	0.8355	0.8903	0.6488
MINT-IQA (Ours)	0.8919	0.9328	0.7224

TABLE IV

ALIGNMENT METRIC PERFORMANCE COMPARISONS ON THE AGIQA-3K DATABASE. THE BEST RESULTS ARE MARKED IN RED AND THE SECOND RESULTS ARE MARKED IN BLUE.

Method	SRCC	PLCC	KRCC
CLIP [20]	0.5972	0.6839	0.4591
HPS [9]	0.6349	0.7000	0.4580
PickScore [14]	0.6977	0.7633	0.5069
ImageReward [15]	0.7298	0.7862	0.5390
StairReward [16]	0.7472	0.8529	0.5554
MINT-IQA (Ours)	0.8749	0.9282	0.7036

to the varying number of evaluation dimensions in the test databases. Since traditional IQA databases have only one dimension for assessment, only one regressor is used for score prediction. The models are implemented with PyTorch and trained on a 40GB NVIDIA RTX A6000 GPU with batch size of 8 on AIGCIQA2023+ database and batch size 16 on the other five databases. The initial learning rate is set to $1e-5$, and decreased using the cosine annealing strategy. We employ Adam optimizer with $\beta_1 = 0.9$ and $\beta_2 = 0.999$.

B. Performance on AIGC IQA Databases

We evaluate the performance of our proposed metric, MINT-IQA, on three recently released AIGC IQA databases including AIGCIQA2023 [17], AGIQA-3K [16], and ImageReward [15]. The performance comparison results are demonstrated in Tables II-V. Handcrafted-based models show poor performance on AIGC IQA databases, indicating that the handcrafted features mainly targeted for natural images are ineffective for evaluating AIGIs. On the other hand, deep learning-based methods achieve relatively better results. However, they are still far away from satisfactory.

MINT-IQA attains state-of-the-art performance across all three AIGC IQA databases, substantially outperforming current IQA models. As shown in Table II, our proposed MINT-IQA model achieves the best performance on our AIGCIQA2023+ from all three perspectives, which demonstrates the effectiveness of MINT-IQA in evaluating human preferences from multiple perspectives. Additionally, as demonstrated in Table III and Table IV, our model outperforms other methods in measuring the quality perception and text-image alignment on AGIQA-3K [16]. This highlights the versatility of our model in understanding human preference for AIGIs

TABLE V

HUMAN PREFERENCE PREDICTION METRIC PERFORMANCE COMPARISONS ON THE IMAGEREWARD DATABASE. PREFERENCE ACCURACY IS CONDUCTED BASED ON THE TEST SET WITH 466 PROMPTS (6,399 COMPARISONS). THE BEST RESULTS ARE MARKED IN RED AND THE SECOND RESULTS ARE MARKED IN BLUE.

Method	Accuracy
CLIP Score [20]	54.82
Aesthetic Score [43]	57.35
BLIP Score [21]	57.76
ImageReward [15]	65.14
MINT-IQA (Ours)	66.46

in terms of both quality perception perspective and alignment perspective.

Our proposed method also shows superior performance on the ImageReward dataset [15] compared to the ImageReward model, as shown in Table V, even though we change the training data format from a single image and its MOS to a pair of images and their comparisons. This further manifests the generalization ability of our model.

C. Performance on Traditional IQA Databases

To further emphasize the effectiveness and generality of our proposed model, we also test it on three traditional large-scale image quality datasets including two technical quality datasets (KonIQ-10k [23], SPAQ [24]) and one aesthetic quality dataset (AVA [25]). From Tables VI-VIII, we first observe that the proposed model achieves the best performance on all three traditional IQA databases. Our method outperforms the current state-of-the-art methods in terms of both SRCC and PLCC. The results indicate that the proposed model has more powerful representation learning abilities in assessing the quality of traditional natural images compared to other handcrafted-based models and deep learning-based models. Although MINT-IQA is designed for assessing the quality of AIGIs, it can also be applied to evaluate the quality real-captured images. It can be observed that our proposed method significantly outperforms other models on the AVA [25] dataset. Note that the number of images in AVA dataset is larger than the other two datasets, so it may be challenging for other models to learn a broadly representative generic feature in such a large-scale dataset. Fortunately, the proposed model can learn the feature representation from a more diverse range of image content in large-scale datasets, which leads to a significant improvement.

D. Visual Question Answering Accuracy

In order to quantitatively measure the capability of our model on explaining human preference for AIGIs. We compare the answers generated by our instruction-tuned model with the other two language models. However, it is hard to directly evaluate the VQA capability based on sentences. To address this issue, we propose to use visual question answering accuracy (VQA_{acc}) for the evaluation of the human preference explanation task, which is computed by directly querying different language models with the same preference-related questions and calculating the accuracy between the model answers and annotations. We evaluate the VQA_{acc} mainly based on the five single-choice questions, three of them from the quality perspective, one from the authenticity perspective, and one from the correspondence perspective.

TABLE VI

RESULTS ON KONIQ-10K DATASET. THE BEST PERFORMANCE RESULTS ARE MARKED IN RED AND THE SECOND-BEST PERFORMANCE RESULTS ARE MARKED IN BLUE.

Method	SRCC	PLCC
BRISQUE [32]	0.665	0.681
ILNIQE [70]	0.507	0.523
HOSA [35]	0.671	0.694
WaDIQaM [40]	0.797	0.805
PQR [71]	0.880	0.884
SFA [72]	0.856	0.872
DBCNN [39]	0.875	0.884
MetaIQA [73]	0.850	0.887
HyperNet [69] (25 crops)	0.906	0.917
MUSIQ [60]	0.916	0.928
TreS [61]	0.907	0.924
LIQE [74]	0.919	0.908
Re-IQA [7]	0.914	0.923
MINT-IQA (Ours)	0.927	0.945

TABLE VII

RESULTS ON SPAQ DATASET. THE BEST PERFORMANCE RESULTS ARE MARKED IN RED AND THE SECOND-BEST PERFORMANCE RESULTS ARE MARKED IN BLUE.

Method	SRCC	PLCC
DIIVINE [75]	0.599	0.600
BRISQUE [32]	0.809	0.817
CORNIA [76]	0.709	0.725
QAC [33]	0.092	0.497
ILNIQE [70]	0.713	0.721
FRIQUEE [77]	0.819	0.830
DBCNN [39]	0.911	0.915
Fang [24] (w/o extra info)	0.908	0.909
MUSIQ [60]	0.917	0.921
Tres [61]	0.915	0.918
LIQE [74]	0.881	-
Re-IQA [7]	0.918	0.925
MINT-IQA (Ours)	0.927	0.932

TABLE VIII

RESULTS ON AVA DATASET. THE BEST PERFORMANCE RESULTS ARE MARKED IN RED AND THE SECOND-BEST PERFORMANCE RESULTS ARE MARKED IN BLUE.

Method	SRCC	PLCC
Kong [30]	0.558	-
NIMA (VGG16) [78]	0.592	0.610
NIMA (Inception-v2) [78]	0.612	0.636
Zeng (ResNet101) [79]	0.719	0.720
Hosu [80] (20 crops)	0.756	0.757
AFDC + SPP (single warp) [81]	0.648	-
AFDC + SPP (4 warps) [81]	0.649	0.671
MUSIQ [60]	0.726	0.738
MINT-IQA (Ours)	0.776	0.783

Given an AI-generated image and its corresponding prompt, there are N_q quality-relevant questions Q_q and answers A_q , N_a authenticity-relevant questions Q_a and their corresponding answers A_a , as well as N_c correspondence-relevant questions Q_c and their corresponding answers A_c . The Q_q , Q_a and Q_c are constructed in the following format:

Q_q : How is the quality of the image?
 Q_a : How is the authenticity of the image?
 Q_c : How is the correspondence between the image and its text prompt?

By feeding the constructed questions (Q_q, Q_a, Q_c) into a large language model, we can get the human preference answer \hat{A} predicted by the LLM. This process can be expressed as

TABLE IX

VQA ACCURACY COMPARISON RESULTS. THE RANDOM ACCURACY IS CALCULATED BASED ON THE NUMBER OF OPTIONS FOR THE SINGLE-CHOICE QUESTIONS. THE BEST RESULTS ARE HIGHLIGHTED IN RED, AND THE SECOND-BEST RESULTS ARE HIGHLIGHTED IN BLUE

VQA _{acc}	Quality	Authenticity	Correspondence
Random	25.0	33.3	33.3
InstructBLIP [55]	8.35	9.08	37.4
Llava [82]	28.3	21.7	45.5
MINT-IQA (Ours)	48.5	57.3	59.4

follows:

$$\hat{A} = \text{LLM}(Q_q, Q_a, Q_c). \quad (6)$$

Since the answers generated by the model are long sentences, we distill the keywords in the generated answers and match them to the corresponding single-choice questions as follows:

$$(\hat{A}_q, \hat{A}_a, \hat{A}_c) = \text{Match}(\text{Distill}(\hat{A}), (Q_q, Q_a, Q_c)), \quad (7)$$

to obtain explicit answers $\hat{A}_q, \hat{A}_a, \hat{A}_c$ for the questions. Then, we separately calculate the average accuracy separately among the N_q quality-relevant questions, N_a authenticity-relevant questions and N_c corresponding-relevant questions for an AI-generated image, and obtain the final VQA_{acc} by computing the mean score for all the K images:

$$\text{VQA}_{\text{acc_Quality}} = \frac{1}{K} \sum_K \left(\frac{1}{N_q} \sum_{N_q} \mathbb{I}(\hat{A}_q = A_q) \right), \quad (8)$$

$$\text{VQA}_{\text{acc_Authenticity}} = \frac{1}{K} \sum_K \left(\frac{1}{N_a} \sum_{N_a} \mathbb{I}(\hat{A}_a = A_a) \right), \quad (9)$$

and

$$\text{VQA}_{\text{acc_Correspondence}} = \frac{1}{K} \sum_K \left(\frac{1}{N_c} \sum_{N_c} \mathbb{I}(\hat{A}_c = A_c) \right), \quad (10)$$

where $\mathbb{I}(a = b) = 1$ if a equals b , and $\mathbb{I}(a = b) = 0$ if a is different from b . In this way, we can measure the performance of the answers generated by language models and evaluate the preference-related understanding capability of these models on AIGIs. As shown in Table IX, compared with the random selection accuracy, InstructBLIP [55], Llava [82], our MINT-IQA model achieves better explanation capability for preference-related questions on AIGIs.

E. Cross-Dataset Evaluation

We further conduct an experiment to test the generalization ability of MINT-IQA in a more challenging cross-dataset setting. Specifically, we train the models on the training set of one database and directly test the generalization ability on the test set of another database. The cross-dataset evaluation experiment is conducted on both the AIGC IQA databases and traditional IQA databases. As shown in Table X, our proposed model MINT-IQA achieves better results compared to latest models TReS [61] for all tasks.

F. Ablation Study

To validate the contributions of the different modules in MINT-IQA, we further conduct ablation studies. The results are demonstrated in Tables XI-XV. We report the averaged SRCC, PLCC, KRCC scores from three perspectives on our AIGCIQA2023+ database for each ablation experiment.

TABLE X

SRCC RESULTS OF CROSS-DATASET VERIFICATION FROM THE QUALITY PERSPECTIVE. **BOLD ENTRIES** INDICATE THE BEST PERFORMERS.

Train on	KonIQ [23]		SPAQ [24]		AGIQA-3K [16](quality)		AIGCIQA2023+ (quality)	
Test on	SPAQ	KonIQ	KonIQ	SPAQ	AIGCIQA2023+	AGIQA-3K	AGIQA-3K	AIGCIQA2023+
TReS [61]	0.765	0.907	0.828	0.915	0.747	0.646	0.634	0.741
MINT-IQA (Ours)	0.772	0.927	0.892	0.927	0.817	0.892	0.770	0.880

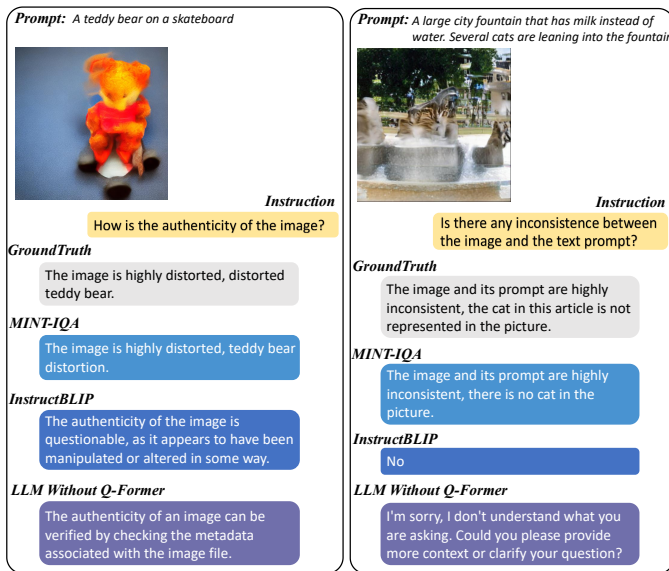


Fig. 11. Ablation study on the vision-language instruction tuning strategy. With fine-tuning on AIGCIQA2023+ database, our proposed model achieves better performance on visual question answering.

1) *Comparison between Different Model Backbone:* To verify the rationality and effectiveness of the Q-Former in the proposed MINT-IQA model, we change the model backbone to CLIP [20] and BLIP [21] for comparison. We directly add our multi-head quality regression to CLIP [20] and BLIP [21], and train them in a similar way. Table XI manifests that our Q-Former based method outperforms conventional CLIP [20] and BLIP [21] as the model backbone.

2) *Comparison between Different Loss Functions:* To further validate the effectiveness of the adopted loss function, we compare it with the cross-entropy loss. We can observe from Table XII that the L1 loss is more effective in dealing with our regression-based IQA tasks.

3) *Comparison between Different Fix Rates:* The training efficiency of a model is crucial in practical applications. Generally, models with fewer active parameters may have better training efficiency but worse performance results. Since the image encoder accounts for the largest proportion of parameters in the model, we conduct ablation experiments to fix some layers of the image encoder. From Table XIII we can observe that freezing the whole model leads to the worst performance, while the fix rate of 0.7 leads to the best performance. It is reasonable since the feature extraction model needs to be trained for this specific task, but due to the dataset size limitation, training the whole model may lead to the overfitting problem. It is also beneficial to consider the balance between the performance and computational efficiency.

4) *Contribution of LLM Segmentation and the Feedback Reward Part:* To verify the effectiveness of the design of the two improvement parts for the performance, we launch further ablation experiments of adding the LLM segmentation module and feedback reward module, and show the results in Table XIV. Using the prompt after LLM Segmentation as the

TABLE XI
ABLATION STUDY ON MODEL BACKBONE.

Backbone	SRCC	PLCC	KRCC
CLIP [20]	0.7086	0.7003	0.5330
BLIP [21]	0.7937	0.7860	0.6038
Q-Former	0.8419	0.8351	0.6432

TABLE XII
ABLATION STUDY ON LOSS FUNCTION.

Loss Function	SRCC	PLCC	KRCC
Cross-entropy	0.7312	0.7199	0.5244
L1 loss	0.8419	0.8351	0.6432

TABLE XIII
ABLATION STUDY ON THE FIX RATE OF IMAGE ENCODER.

Fix Rate	SRCC	PLCC	KRCC	GPU Memory
1.0	0.8235	0.8190	0.6229	9450M
0.8	0.8374	0.8325	0.6372	14846M
0.7	0.8419	0.8351	0.6432	17586M
0.6	0.8411	0.8346	0.6417	20336M
0.5	0.8403	0.8338	0.6398	22330M

TABLE XIV
IMPROVEMENTS OF LLM SEGMENTATION AND FEEDBACK REWARD.

Segmentation	SRCC	PLCC	KRCC
MINT-IQA (Ours)	0.8419	0.8351	0.6432
+ LLM Seg.	0.8456	0.8400	0.6482
+ Reward	0.8499	0.8447	0.6539
+ LLM Seg. + Reward	0.8510	0.8453	0.6546

TABLE XV
ABLATION STUDY ON ZERO CONVOLUTION CONNECTION. VQA ACCURACY IS FROM THE TEST SET OF 480 IMAGES AND 2400 DETAILED EXPLANATIONS.

Zero Conv	Quality	Authenticity	Correspondence
without	47.2	54.4	57.1
with	48.5	57.3	59.4

input leads to better performance than raw prompt. The reward feedback part can also further improve the performance of our model. Moreover, the combination of two further improved modules achieves better results compared to only using one part. This could suggest that more granular input processing and dynamic adjustment of evaluation metrics based on explanatory feedback can lead to a more accurate alignment with human preference judgement.

5) *Contribution of zero convolution:* Table XV validates the significance of initializing the connection part between the two Q-Formers with zero convolution. The removal of the connection between two Q-Formers through zero convolution leads to poorer performance. This highlights the effectiveness of inserting the scoring features into the explanation module for better VQA performance.

6) *Contribution of the vision-language instruction tuning strategy:* Finally, we investigate the impact of the vision-language instruction tuning strategy, and show the results in Fig. 11. The answers generated without fine-tuning on our AIGCIQA2023+ database show poor consistency with human preference. If we further remove the connection between the Q-Former and the LLM, the answer performance drop is much more severe. This further highlights the value of vision-language instruction tuning strategy in aligning AI-generated responses with human preferences.

VI. CONCLUSION

This work aims to better understand and evaluate human visual preferences for AIGIs. We extend the AIGCIQA2023 database to AIGCIQA2023+, which includes more fine-grained preference labels from the perspectives of quality, authenticity, and text-image correspondence. The experimental analysis demonstrates that these three dimensions can reflect different aspects of human visual preferences on AIGIs, which further manifests the evaluation of Quality of Experience (QoE) for AIGIs should be considered from multiple dimensions. Based on the constructed database, we propose a novel method termed MINT-IQA, which allows for a more comprehensive evaluation of the human preferences for AIGIs from multiple perspectives, and gives fine-grained explanations for the preference-related questions. Extensive experimental results demonstrate the effectiveness of MINT-IQA on both preference evaluation and explanation for AIGIs.

REFERENCES

- [1] A. Ramesh, M. Pavlov, G. Goh, S. Gray, C. Voss, A. Radford, M. Chen, and I. Sutskever, "Zero-shot text-to-image generation," in *International Conference on Machine Learning (ICML)*, 2021, pp. 8821–8831.
- [2] R. Rombach, A. Blattmann, D. Lorenz, P. Esser, and B. Ommer, "High-Resolution Image Synthesis with Latent Diffusion Models," *Proceedings of the IEEE/CVF Conference on Computer Vision and Pattern Recognition (CVPR)*, pp. 10 674–10 685, 2022.
- [3] F. Bao, S. Nie, K. Xue, C. Li, S. Pu, Y. Wang, G. Yue, Y. Cao, H. Su, and J. Zhu, "One transformer fits all distributions in multi-modal diffusion at scale," *arXiv preprint arXiv:2303.06555*, 2023.
- [4] H. R. Sheikh, M. F. Sabir, and A. C. Bovik, "A statistical evaluation of recent full reference image quality assessment algorithms," *IEEE Transactions on Image Processing (TIP)*, pp. 3440–3451, 2006.
- [5] S. Wang, K. Gu, S. Ma, and W. Gao, "Joint chroma downsampling and upsampling for screen content image," *IEEE Transactions on Circuits and Systems for Video Technology (TCSVT)*, pp. 1595–1609, 2015.
- [6] Z. Ying, H. Niu, P. Gupta, D. Mahajan, D. Ghadiyaram, and A. Bovik, "From patches to pictures (paq-2-piq): Mapping the perceptual space of picture quality," in *Proceedings of the IEEE/CVF Conference on Computer Vision and Pattern Recognition (CVPR)*, 2020, pp. 3575–3585.
- [7] A. Saha, S. Mishra, and A. C. Bovik, "Re-iqa: Unsupervised learning for image quality assessment in the wild," in *Proceedings of the IEEE/CVF Conference on Computer Vision and Pattern Recognition (CVPR)*, 2023, pp. 5846–5855.
- [8] H. Duan, W. Shen, X. Min, Y. Tian, J.-H. Jung, X. Yang, and G. Zhai, "Develop then rival: A human vision-inspired framework for superimposed image decomposition," *IEEE Transactions on Multimedia (TMM)*, 2022.
- [9] X. Wu, K. Sun, F. Zhu, R. Zhao, and H. Li, "Better aligning text-to-image models with human preference," *arXiv preprint arXiv:2303.14420*, 2023.
- [10] L. Yang, H. Duan, L. Teng, Y. Zhu, X. Liu, M. Hu, X. Min, G. Zhai, and P. L. Callet, "Aigcoiqa2024: Perceptual quality assessment of ai generated omnidirectional images," *arXiv preprint arXiv:2404.01024*, 2024.
- [11] K. Ding, K. Ma, S. Wang, and E. P. Simoncelli, "Image quality assessment: Unifying structure and texture similarity," *IEEE Transactions on Pattern Analysis and Machine Intelligence (TPAMI)*, vol. 44, no. 5, pp. 2567–2581, 2020.
- [12] K. Lee, H. Liu, M. Ryu, O. Watkins, Y. Du, C. Boutilier, P. Abbeel, M. Ghavamzadeh, and S. S. Gu, "Aligning text-to-image models using human feedback," *arXiv preprint arXiv:2302.12192*, 2023.
- [13] T. Zhou, S. Tan, W. Zhou, Y. Luo, Y.-G. Wang, and G. Yue, "Adaptive mixed-scale feature fusion network for blind ai-generated image quality assessment," *IEEE Transactions on Broadcasting*, 2024.
- [14] Y. Kirstain, A. Polyak, U. Singer, S. Matiana, J. Penna, and O. Levy, "Pick-a-pic: An open dataset of user preferences for text-to-image generation," *arXiv preprint arXiv:2305.01569*, 2023.
- [15] J. Xu, X. Liu, Y. Wu, Y. Tong, Q. Li, M. Ding, J. Tang, and Y. Dong, "Imagereward: Learning and evaluating human preferences for text-to-image generation," *arXiv preprint arXiv:2304.05977*, 2023.
- [16] C. Li, Z. Zhang, H. Wu, W. Sun, X. Min, X. Liu, G. Zhai, and W. Lin, "Aigciqa-3k: An open database for ai-generated image quality assessment," *arXiv preprint arXiv:2306.04717*, 2023.
- [17] J. Wang, H. Duan, J. Liu, S. Chen, X. Min, and G. Zhai, "Aigciqa2023: A large-scale image quality assessment database for ai generated images: from the perspectives of quality, authenticity and correspondence," in *CAAI International Conference on Artificial Intelligence (ICAI)*, 2023, pp. 46–57.
- [18] I. Gulrajani, F. Ahmed, M. Arjovsky, V. Dumoulin, and A. C. Courville, "Improved training of wasserstein gans," *Proceedings of the Advances in Neural Information Processing Systems (NeurIPS)*, 2017.
- [19] M. Heusel, H. Ramsauer, T. Unterthiner, B. Nessler, and S. Hochreiter, "Gans trained by a two time-scale update rule converge to a local nash equilibrium," *Proceedings of the Advances in Neural Information Processing Systems (NeurIPS)*, 2017.
- [20] A. Radford, J. W. Kim, C. Hallacy, A. Ramesh, G. Goh, S. Agarwal, G. Sastry, A. Askell, P. Mishkin, J. Clark *et al.*, "Learning transferable visual models from natural language supervision," in *International Conference on Machine Learning (ICML)*, 2021, pp. 8748–8763.
- [21] J. Li, D. Li, C. Xiong, and S. Hoi, "Blip: Bootstrapping language-image pre-training for unified vision-language understanding and generation," in *International Conference on Machine Learning (ICML)*, 2022, pp. 12 888–12 900.
- [22] T. Virtanen, M. Nuutinen, M. Vaahteranoksa, P. Oittinen, and J. Häkkinen, "Cid2013: A database for evaluating no-reference image quality assessment algorithms," *IEEE Transactions on Image Processing (TIP)*, pp. 390–402, 2014.
- [23] V. Hosu, H. Lin, T. Sziranyi, and D. Saupe, "Koniq-10k: An ecologically valid database for deep learning of blind image quality assessment," *IEEE Transactions on Image Processing (TIP)*, pp. 4041–4056, 2020.
- [24] Y. Fang, H. Zhu, Y. Zeng, K. Ma, and Z. Wang, "Perceptual quality assessment of smartphone photography," in *Proceedings of the IEEE/CVF Conference on Computer Vision and Pattern Recognition (CVPR)*, 2020, pp. 3677–3686.
- [25] N. Murray, L. Marchesotti, and F. Perronnin, "AVA: A large-scale database for aesthetic visual analysis," *Proceedings of the IEEE/CVF Conference on Computer Vision and Pattern Recognition (CVPR)*, pp. 2408–2415, 2012.
- [26] Z. J. Wang, E. Montoya, D. Munechika, H. Yang, B. Hoover, and D. H. Chau, "Diffusiondb: A large-scale prompt gallery dataset for text-to-image generative models," *arXiv preprint arXiv:2210.14896*, 2022.
- [27] X. Min, H. Duan, W. Sun, Y. Zhu, and G. Zhai, "Perceptual video quality assessment: A survey," *arXiv preprint arXiv:2402.03413*, 2024.
- [28] H. Duan, X. Min, W. Sun, Y. Zhu, X.-P. Zhang, and G. Zhai, "Attentive deep image quality assessment for omnidirectional stitching," *IEEE Journal of Selected Topics in Signal Processing (J-STSP)*, 2023.
- [29] H. Duan, X. Zhu, Y. Zhu, X. Min, and G. Zhai, "A quick review of human perception in immersive media," *IEEE Open Journal on Immersive Displays (OJID)*, 2024.
- [30] S. Kong, X. Shen, Z. Lin, R. Mech, and C. Fowlkes, "Photo aesthetics ranking network with attributes and content adaptation," in *European Conference on Computer Vision (ECCV)*, 2016, pp. 662–679.
- [31] A. Mittal, R. Soundararajan, and A. C. Bovik, "Making a "completely blind" image quality analyzer," *IEEE Signal Processing Letters*, pp. 209–212, 2012.
- [32] A. Mittal, A. K. Moorthy, and A. C. Bovik, "No-reference image quality assessment in the spatial domain," *IEEE Transactions on Image Processing (TIP)*, pp. 4695–4708, 2012.
- [33] W. Xue, L. Zhang, and X. Mou, "Learning without human scores for blind image quality assessment," in *Proceedings of the IEEE/CVF Conference on Computer Vision and Pattern Recognition (CVPR)*, 2013, pp. 995–1002.
- [34] X. Min, G. Zhai, K. Gu, Y. Liu, and X. Yang, "Blind image quality estimation via distortion aggravation," *IEEE Transactions on Broadcasting (TBC)*, pp. 508–517, 2018.
- [35] J. Xu, P. Ye, Q. Li, H. Du, Y. Liu, and D. Doermann, "Blind image quality assessment based on high order statistics aggregation," *IEEE Transactions on Image Processing (TIP)*, pp. 4444–4457, 2016.
- [36] X. Min, K. Gu, G. Zhai, J. Liu, X. Yang, and C. W. Chen, "Blind quality assessment based on pseudo-reference image," *IEEE Transactions on Multimedia (TMM)*, pp. 2049–2062, 2017.
- [37] D. Kundu, D. Ghadiyaram, A. C. Bovik, and B. L. Evans, "Large-scale crowdsourced study for tone-mapped hdr pictures," *IEEE Transactions on Image Processing (TIP)*, pp. 4725–4740, 2017.
- [38] L. Kang, P. Ye, Y. Li, and D. Doermann, "Convolutional neural networks for no-reference image quality assessment," in *Proceedings of the*

- IEEE/CVF Conference on Computer Vision and Pattern Recognition (CVPR)*, 2014, pp. 1733–1740.
- [39] W. Zhang, K. Ma, J. Yan, D. Deng, and Z. Wang, “Blind image quality assessment using a deep bilinear convolutional neural network,” *IEEE Transactions on Circuits and Systems for Video Technology (TCSVT)*, pp. 36–47, 2018.
- [40] S. Bosse, D. Maniry, K.-R. Müller, T. Wiegand, and W. Samek, “Deep neural networks for no-reference and full-reference image quality assessment,” *IEEE Transactions on Image Processing (TIP)*, pp. 206–219, 2017.
- [41] W. Sun, X. Min, D. Tu, S. Ma, and G. Zhai, “Blind quality assessment for in-the-wild images via hierarchical feature fusion and iterative mixed database training,” *IEEE Journal of Selected Topics in Signal Processing (J-STSP)*, 2023.
- [42] Y. Li, H. Fan, R. Hu, C. Feichtenhofer, and K. He, “Scaling language-image pre-training via masking,” in *Proceedings of the IEEE/CVF Conference on Computer Vision and Pattern Recognition (CVPR)*, 2023, pp. 23 390–23 400.
- [43] C. Schuhmann, R. Beaumont, R. Vencu, C. Gordon, R. Wightman, M. Cherti, T. Coombes, A. Katta, C. Mullis, M. Wortsman *et al.*, “Laion-5b: An open large-scale dataset for training next generation image-text models,” *Advances in Neural Information Processing Systems (NeurIPS)*, pp. 25 278–25 294, 2022.
- [44] A. Nichol, P. Dhariwal, A. Ramesh, P. Shyam, P. Mishkin, B. McGrew, I. Sutskever, and M. Chen, “Glide: Towards photorealistic image generation and editing with text-guided diffusion models,” *International Conference on Machine Learning (ICML)*, pp. 16 784–16 804, 2021.
- [45] Y. Zhou, R. Zhang, C. Chen, C. Li, C. Tensmeyer, T. Yu, J. Gu, J. Xu, and T. Sun, “Towards language-free training for text-to-image generation,” in *Proceedings of the IEEE/CVF Conference on Computer Vision and Pattern Recognition (CVPR)*, June 2022, pp. 17 907–17 917.
- [46] A. Ramesh, P. Dhariwal, A. Nichol, C. Chu, and M. Chen, “Hierarchical text-conditional image generation with clip latents,” *arXiv preprint arXiv:2204.06125*, 2022.
- [47] R. Rombach, A. Blattmann, D. Lorenz, P. Esser, and B. Ommer, “High-resolution image synthesis with latent diffusion models,” *Proceedings of the IEEE/CVF Conference on Computer Vision and Pattern Recognition (CVPR)*, pp. 10 674–10 685, 2021.
- [48] L. Zhang and M. Agrawala, “Adding conditional control to text-to-image diffusion models,” *arXiv preprint arXiv:2302.05543*, 2023.
- [49] J. Yu, Y. Xu, J. Y. Koh, T. Luong, G. Baid, Z. Wang, V. Vasudevan, A. Ku, Y. Yang, B. K. Ayan *et al.*, “Scaling autoregressive models for content-rich text-to-image generation,” *arXiv preprint arXiv:2206.10789*, 2022.
- [50] H. Duan, X. Min, Y. Zhu, G. Zhai, X. Yang, and P. Le Callet, “Confusing image quality assessment: Toward better augmented reality experience,” *IEEE Transactions on Image Processing (TIP)*, pp. 7206–7221, 2022.
- [51] Y. Fang, W. Wang, B. Xie, Q. Sun, L. Wu, X. Wang, T. Huang, X. Wang, and Y. Cao, “Eva: Exploring the limits of masked visual representation learning at scale,” in *Proceedings of the IEEE/CVF Conference on Computer Vision and Pattern Recognition (CVPR)*, 2023, pp. 19 358–19 369.
- [52] Y. Sun, X. Min, H. Duan, and G. Zhai, “How is visual attention influenced by text guidance? database and model,” *arXiv preprint arXiv:2404.07537*, 2024.
- [53] H. Duan, W. Shen, X. Min, D. Tu, J. Li, and G. Zhai, “Saliency in augmented reality,” in *Proceedings of the 30th ACM International Conference on Multimedia (ACM MM)*, 2022, pp. 6549–6558.
- [54] J. Li, D. Li, S. Savarese, and S. Hoi, “Blip-2: Bootstrapping language-image pre-training with frozen image encoders and large language models,” *arXiv preprint arXiv:2301.12597*, 2023.
- [55] W. Dai, J. Li, D. Li, A. M. H. Tiong, J. Zhao, W. Wang, B. Li, P. Fung, and S. Hoi, “Instructblip: Towards general-purpose vision-language models with instruction tuning,” *arXiv preprint arXiv:2305.06500*, 2023.
- [56] L. Zheng, W.-L. Chiang, Y. Sheng, S. Zhuang, Z. Wu, Y. Zhuang, Z. Lin, Z. Li, D. Li, E. Xing *et al.*, “Judging llm-as-a-judge with mt-bench and chatbot arena,” *arXiv preprint arXiv:2306.05685*, 2023.
- [57] H. Touvron, T. Lavril, G. Izacard, X. Martinet, M.-A. Lachaux, T. Lacroix, B. Rozière, N. Goyal, E. Hambro, F. Azhar *et al.*, “Llama: Open and efficient foundation language models,” *arXiv preprint arXiv:2302.13971*, 2023.
- [58] K. Simonyan and A. Zisserman, “Very deep convolutional networks for large-scale image recognition,” *arXiv preprint arXiv:1409.1556*, 2014.
- [59] K. He, X. Zhang, S. Ren, and J. Sun, “Deep residual learning for image recognition,” in *Proceedings of the IEEE/CVF Conference on Computer Vision and Pattern Recognition (CVPR)*, 2016, pp. 770–778.
- [60] J. Ke, Q. Wang, Y. Wang, P. Milanfar, and F. Yang, “Musiq: Multi-scale image quality transformer,” in *Proceedings of the IEEE/CVF International Conference on Computer Vision (ICCV)*, 2021, pp. 5148–5157.
- [61] S. A. Golestaneh, S. Dadsetan, and K. M. Kitani, “No-reference image quality assessment via transformers, relative ranking, and self-consistency,” in *Proceedings of the IEEE/CVF Winter Conference on Applications of Computer Vision (WACV)*, 2022, pp. 1220–1230.
- [62] J. Wang, K. C. Chan, and C. C. Loy, “Exploring clip for assessing the look and feel of images,” in *AAAI*, 2023.
- [63] J. Yan, J. Li, and X. Fu, “No-reference quality assessment of contrast-distorted images using contrast enhancement,” *arXiv preprint arXiv:1904.08879*, 2019.
- [64] N. D. Narvekar and L. J. Karam, “A no-reference perceptual image sharpness metric based on a cumulative probability of blur detection,” in *International Workshop on Quality of Multimedia Experience (QoMEX)*, 2009, pp. 87–91.
- [65] K. Gu, G. Zhai, X. Yang, and W. Zhang, “Hybrid no-reference quality metric for singly and multiply distorted images,” *IEEE Transactions on Broadcasting (TBC)*, pp. 555–567, 2014.
- [66] T. Salimans, I. J. Goodfellow, W. Zaremba, V. Cheung, A. Radford, and X. Chen, “Improved techniques for training gans,” *ArXiv preprint arXiv:1606.03498*, 2016.
- [67] M. Bińkowski, D. J. Sutherland, M. Arbel, and A. Gretton, “Demystifying mmd gans,” *arXiv preprint arXiv:1801.01401*, 2018.
- [68] W. Xue, X. Mou, L. Zhang, A. C. Bovik, and X. Feng, “Blind image quality assessment using joint statistics of gradient magnitude and laplacian features,” *IEEE Transactions on Image Processing (TIP)*, pp. 4850–4862, 2014.
- [69] S. Su, Q. Yan, Y. Zhu, C. Zhang, X. Ge, J. Sun, and Y. Zhang, “Blindly assess image quality in the wild guided by a self-adaptive hyper network,” in *Proceedings of the IEEE/CVF Conference on Computer Vision and Pattern Recognition (CVPR)*, 2020, pp. 3667–3676.
- [70] L. Zhang, L. Zhang, and A. C. Bovik, “A feature-enriched completely blind image quality evaluator,” *IEEE Transactions on Image Processing (TIP)*, pp. 2579–2591, 2015.
- [71] H. Zeng, L. Zhang, and A. C. Bovik, “A probabilistic quality representation approach to deep blind image quality prediction,” *arXiv preprint arXiv:1708.08190*, 2017.
- [72] D. Li, T. Jiang, W. Lin, and M. Jiang, “Which has better visual quality: The clear blue sky or a blurry animal?” *IEEE Transactions on Multimedia (TMM)*, pp. 1221–1234, 2018.
- [73] H. Zhu, L. Li, J. Wu, W. Dong, and G. Shi, “Metaiqa: deep meta-learning for no-reference image quality assessment,” in *Proceedings of the IEEE/CVF Conference on Computer Vision and Pattern Recognition (CVPR)*, 2020, pp. 14 143–14 152.
- [74] W. Zhang, G. Zhai, Y. Wei, X. Yang, and K. Ma, “Blind image quality assessment via vision-language correspondence: A multitask learning perspective,” in *Proceedings of the IEEE/CVF Conference on Computer Vision and Pattern Recognition (CVPR)*, 2023, pp. 14 071–14 081.
- [75] A. K. Moorthy and A. C. Bovik, “Blind image quality assessment: From natural scene statistics to perceptual quality,” *IEEE Transactions on Image Processing (TIP)*, pp. 3350–3364, 2011.
- [76] P. Ye, J. Kumar, L. Kang, and D. Doermann, “Unsupervised feature learning framework for no-reference image quality assessment,” in *Proceedings of the IEEE/CVF Conference on Computer Vision and Pattern Recognition (CVPR)*, 2012, pp. 1098–1105.
- [77] D. Ghadiyaram and A. C. Bovik, “Perceptual quality prediction on authentically distorted images using a bag of features approach,” *Journal of Vision (JOV)*, pp. 32–32, 2017.
- [78] H. Talebi and P. Milanfar, “Nima: Neural image assessment,” *IEEE Transactions on Image Processing (TIP)*, pp. 3998–4011, 2018.
- [79] H. Zeng, Z. Cao, L. Zhang, and A. C. Bovik, “A unified probabilistic formulation of image aesthetic assessment,” *IEEE Transactions on Image Processing (TIP)*, pp. 1548–1561, 2019.
- [80] V. Hosu, B. Goldlucke, and D. Sauppe, “Effective aesthetics prediction with multi-level spatially pooled features,” in *Proceedings of the IEEE/CVF Conference on Computer Vision and Pattern Recognition (CVPR)*, 2019, pp. 9375–9383.
- [81] Q. Chen, W. Zhang, N. Zhou, P. Lei, Y. Xu, Y. Zheng, and J. Fan, “Adaptive fractional dilated convolution network for image aesthetics assessment,” in *Proceedings of the IEEE/CVF Conference on Computer Vision and Pattern Recognition (CVPR)*, 2020, pp. 14 114–14 123.
- [82] H. Liu, C. Li, Q. Wu, and Y. J. Lee, “Visual instruction tuning,” *Proceedings of the Advances in Neural Information Processing Systems (NeurIPS)*, 2023.